Characterizing Drying in the South American Monsoon Onset Season with the Moist Static Energy Budget

JANE E. SMYTH AND YI MING[a]

Program in Atmospheric and Oceanic Sciences, Princeton University, Princeton, New Jersey

(Manuscript received 25 March 2020, in final form 21 July 2020)

ABSTRACT: The tropical atmospheric circulation and attendant rainfall exhibit seasonally dependent responses to increasing temperatures. Understanding changes in the South American monsoon system is of particular interest given the sensitivity of the southern Amazon rainforest to changes in dry season length. We utilize the latest Geophysical Fluid Dynamics Laboratory Atmospheric Model (GFDL AM4) to analyze the response of the South American monsoon to uniform sea surface temperature (SST) warming. SST warming is a poorly understood yet impactful component of greenhouse gas–induced climate change. Region-mean rainfall declines by 11%, and net precipitation (precipitation minus evaporation) declines by 40%, during the monsoon onset season (September–November), producing a more severe dry season. The column-integrated moist static energy (MSE) budget helps elucidate the physical mechanisms of the simulated drying. Based on the seasonal analysis, precipitation reductions tend to occur when 1) a convecting region's climatological MSE export is dominated by horizontal rather than vertical advection, and 2) the horizontal MSE advection increases in the perturbed climate, impeding ascent. On a synoptic scale, the South American low-level jet strengthens and exports more moisture from the monsoon sector, exacerbating spring drying.

KEYWORDS: Amazon region; Tropics; Dynamics; Monsoons; Precipitation; Climate change

1. Introduction

The physical factors controlling the tropical precipitation distribution remain poorly characterized, especially on regional scales. This incomplete theoretical understanding impedes efforts to predict the precipitation response to climate change (e.g., Xie et al. 2015; Kent et al. 2015; Chou and Neelin 2004). The challenge is particularly salient over land, where economies and ecosystems are sensitive to changes in rainfall characteristics (amount, intensity, seasonal cycle, etc.) (e.g., Byrne and O'Gorman 2015; Hill 2019). In South America, climate change–induced rainfall reductions could destabilize the Amazon rainforest ecosystem, agriculture, and the hydropower-based Brazilian electricity system, among other impacts (Boisier et al. 2015; Ruffato-Ferreira et al. 2017).

The monsoon regions spanning the tropics are characterized by abrupt transitions from dry to rainy seasons and receive most of their annual precipitation in local summer. The seasonal transitions depend on local meridional moist static energy (MSE) gradients, where higher near-surface MSE favors convection and rainfall (Emanuel 1995; Privé and Plumb 2007; Seth et al. 2019). In six global monsoon systems, interannual precipitation variability is strongly correlated with low-level MSE anomalies poleward of the climatological maximum (Hurley and Boos 2013). Advances in relating the location of the intertropical convergence zone (ITCZ) to interhemispheric energy imbalances have also shed light on monsoonal behavior (Kang et al. 2008; Schneider et al. 2014; Heaviside and Czaja 2013). However, the distinct behavior of land monsoons and adjacent oceanic ITCZ over the seasonal cycle, interannually, and in response to orbital forcing underscores the importance of zonal asymmetry in the tropics (Adam et al. 2016; Boos and Korty 2016; Smyth et al. 2018). Numerous authors therefore advocate for an adaptation of the zonal mean energetic framework to account for zonal inhomogeneities (Muller and O'Gorman 2011; Boos and Korty 2016; Biasutti et al. 2018).

The South American monsoon system sustains a large section of the world's largest rainforest: the Amazon. The dry season length plays a limiting role in rainforest survival, such that rainfall reductions in this season are more ecologically consequential than comparable changes during the wet season (Fu and Li 2004). Given its relatively long dry season, the South American monsoon sector is vulnerable to reductions in soil moisture and susceptible to a rainforest–savanna ecosystem transition (Boisier et al. 2015; Fu et al. 2013). The Amazon rainforest plays an outsized role in the global carbon cycle, accounting for a quarter of the global forest carbon uptake of 2.4 billion metric tons per year (Kintisch 2015). Therefore, beyond the loss of biodiversity, such an ecosystem transition would increase atmospheric CO_2 globally (Fu et al. 2013).

Over South America, there is not a clear understanding of how precipitation will change with global warming. CMIP3 A1B scenario simulations, which reflect a path to rapid economic growth with a balanced use of energy sources, show disagreement among models with no statistically significant ensemble mean change over South America, while studies of the CMIP5 suite indicate the possibility of severe drying in the annual mean and rainy season (Vera et al. 2006; Li et al. 2006; Torres and Marengo 2013; Lee and Wang 2014). On the other hand, 9 of 10 CMIP5 model historical runs indicate a trend of increased rainy season duration over the monsoon sector

[a] Current affiliation: Geophysical Fluid Dynamics Laboratory/NOAA, Princeton, New Jersey.

Corresponding author: Jane E. Smyth, jsmyth@princeton.edu

DOI: 10.1175/JCLI-D-20-0217.1

(Jones and Carvalho 2013). These disparate conclusions can be attributed to differing parameterizations of key convective, cloud, and land processes in models, and uncertainty regarding model-simulated sea surface temperature (SST) changes (Li et al. 2006).

Despite the aforementioned issues, some aspects of how the seasonal cycle of precipitation will respond to increased atmospheric CO_2 are well characterized. Based on CMIP3, CMIP5, and CMIP6 simulations, higher CO_2 leads to an increased amplitude in the seasonal cycle of precipitation (Chou and Lan 2012; Dwyer et al. 2014; Wang et al. 2020), a phase shift such that rainfall is inhibited in spring and enhanced later in the rainy season (Biasutti and Sobel 2009; Seth et al. 2011, 2013), and a longer dry season over land (Lau et al. 2013; Boisier et al. 2015), at least in the Southern Hemisphere monsoon sectors (Wang et al. 2020). Further supporting the latter conclusion, and counter to the results of Jones and Carvalho (2013), Fu et al. (2013) report an observed trend of lengthening dry seasons over southern Amazonia between 1979 and 2011. They link the extended dry season with increased convective inhibition: surface relative humidity has declined over the Amazon due to increasing surface temperatures and insufficient surface moisture sources. Such observations portend further drying as the climate warms. Since rainforests are much less prevalent in regions where the dry season length exceeds 3 months (with dry month precipitation less than 2 mm day^{-1}), the rainforest area is expected to diminish with surface warming (Boisier et al. 2015).

The literature outlined above demonstrates a growing consensus that southern Amazonia may be subject to substantial changes in hydroclimate as temperatures increase. However, given the focus on observational data and output from fully coupled models forced with complicated emissions scenarios, it has been difficult to establish definitive physical explanations for these results. Simplified model experiments enable one to better identify and understand the mechanisms of precipitation change. Insights from these studies can elucidate results from more realistic modeling experiments and the observational record, and build (or erode) confidence in the coupled model projections. This study was conceived to work toward that end.

To approach this aim, the study draws on the MSE budget theoretical framework, background on which will be provided in the following section. The analysis focuses on how the climatological MSE budget regulation relates to the hydrological response to SST warming, with a chief interest in how this relationship varies seasonally over the monsoon sector. While the MSE theory is diagnostic in nature, establishing how the budget regulation relates to forced hydrological changes might inform a prognostic theory. In addition, the study examines how synoptic circulation changes may contribute to the South American hydrological response to warming. The overarching goal of the study is to gain mechanistic insights that will aid interpretation of CMIP model experiments and observations, ultimately informing climate projections.

2. Experimental design

a. *Model experiments*

We utilize two simulations performed with the latest Geophysical Fluid Dynamics Laboratory (GFDL) atmospheric general circulation model, AM4. AM4's cubed-sphere dynamical core avoids polar singularities and reduces the size variation of grid boxes, among other benefits. Compared to previous generations of GFDL models, it features improved resolution (~100 km; 33 vertical levels), a double plume model representing shallow and deep convection, and updated radiative transfer code. For more details on the model formulation, the reader is referred to Zhao et al. (2018a,b).

The control simulation is forced with a monthly varying climatology of observed gridded SSTs and sea ice concentrations (1979–2014) from Taylor et al. (2000); global monthly mean concentrations of greenhouse gases (GHGs), ozone-depleting substances, and emissions from the year 2010; and a fixed seasonal cycle of vegetation (Zhao et al. 2018b).

In the experimental simulation, the prescribed SST field is uniformly warmed by 2 K at all times (Cess et al. 1990). SSTs exert a strong if not dominant influence on precipitation variability in monsoon regions (Hurley and Boos 2013). For example, previous studies succeeded in simulating the late twentieth-century Sahel drought given the time series of observed SSTs (Giannini et al. 2003; Lu and Delworth 2005). Determining how the SST changes associated with global warming modulate precipitation is therefore a practical first step toward understanding the full response. This problem can be made more tractable by decomposing the anomalous SST field into uniform and spatially varying components (Chadwick 2016; Hill et al. 2015, 2017). Uniform SST warming experiments therefore allow one to better understand the full climate response in coupled models (e.g., Held et al. 2005). A uniform 2-K perturbation experiment is an appealing idealization for multiple reasons. First, mean SST warming is a robust response to rising greenhouse gas levels. Second, over tropical land areas, the precipitation response to SST changes and its intermodel uncertainty are both dominated by the response to the uniform warming component (Chadwick 2016; He et al. 2014; Held et al. 2005; Hill et al. 2017). Previous studies utilizing uniform SST warming simulations to assess changes in the seasonality of tropical precipitation consider the zonal mean exclusively (Huang et al. 2013; Dwyer et al. 2014). The present work builds on these studies by focusing on regional precipitation changes and utilizing the MSE budget framework to interpret results.

Uniform SST warming experiments exclude, by design, the influence of changing SST patterns, vegetation, and CO_2 radiative effects. This simplification facilitates mechanistic analysis because hydrological changes can be attributed to a spatially and temporally uniform change in the lower boundary condition. If a precipitation response is common to the uniform SST warming experiment and more realistic high-CO_2 experiments (e.g., Biasutti et al. 2009; Seth et al. 2011, 2013; Wang et al. 2020), it is likely a robust response to warming. Where the realistic high-CO_2 experiment differs, some other aspect of the climate response to greenhouse gas emissions opposes that elicited by uniform warming. Further experiments would be needed to diagnose the underlying driver (e.g., anomalous SST gradients, direct CO_2 effects, ocean dynamics), and the credibility of the projection depends on our confidence in that aspect of the simulation.

Each simulation was run for 21 years generating daily output, with the first year considered as spinup initialization and removed for the analyses. Given the sensitivities of the Amazon rainforest to changes in the dry season amplitude and length described in section 1, we focus on the austral spring season (September–November), when the dry season terminates and the monsoon system develops.

b. Moist static energy budget theory

The MSE budget serves as the principal theoretical framework in our analysis of monsoon rainfall. The MSE or h is defined as $h = c_pT + gz + L_vq - L_fq_{\text{ice}}$, where c_p is the heat capacity of air at constant pressure, T is temperature, g is the gravitational constant, z is geopotential height, L_v is the latent heat of vaporization of water, q is specific humidity, L_f is the latent heat of fusion of water, and q_{ice} is specific mass of ice. The column-integrated MSE budget is given by

$$\frac{\partial}{\partial t}\{\overline{\mathscr{E}}\} + \{\overline{\mathbf{v}} \cdot \nabla_p \overline{h}\} + \left\{\overline{\omega}\frac{\partial \overline{h}}{\partial p}\right\} + \nabla \cdot \{\overline{h'\mathbf{v}'}\} \approx \overline{F}_{\text{net}}. \quad (1)$$

The curly braces represent column integrals, $\mathscr{E}$ is the internal energy, $\mathbf{v}$ is the horizontal wind vector, ∇_p is the horizontal gradient operator on constant pressure surfaces, ω is vertical velocity in pressure coordinates, and $\overline{F}_{\text{net}}$ is the total of surface and top-of-atmosphere (TOA) radiative fluxes and surface turbulent fluxes, signed positive into the atmosphere. Overbars denote time means, and primes are temporal deviations. The advantage of an MSE perspective over a moisture budget approach is that through cancellation of large terms in the vertically integrated thermodynamic and moisture equations, column MSE variations are directly linked to surface and TOA energy fluxes (Neelin 2007). Further, over land on climatic time scales, the net surface fluxes are zero, so only TOA fluxes need to be considered.

Neelin and Held (1987) first popularized an MSE budget perspective for the purposes of understanding tropical precipitation. They developed a simple two-layer model assuming no transients and small horizontal MSE gradients, and therefore a dominant balance of $\overline{F}_{\text{net}} \approx \{\overline{\omega}\,\partial\overline{h}/\partial p\}$. They defined the gross moist stability (GMS) as the MSE difference between the upper and lower layers, essentially the energetic stratification of the atmosphere. Based on this model, one expects precipitation where the GMS is small and positive, signaling MSE export by deep moist convection.

In reality, there exist precipitating tropical regions with negative GMS (essentially $\{\overline{\omega}\,\partial\overline{h}/\partial p\} < 0$) such as the eastern Pacific ITCZ sector (Back and Bretherton 2006). Given the midtropospheric minimum of the typical vertical MSE profile, shallow precipitating convection imports MSE to the column. In such regions, horizontal MSE advection is the primary process balancing energy input F_{net}. With its simplifying assumptions, the Neelin–Held theory cannot predict precipitating circulations in a negative GMS regime such as this. Furthermore, the Coriolis parameter is small in the tropics, and pressure gradients are rapidly smoothed by gravity waves. This ensures weak temperature gradients in the free troposphere (Charney 1963). Thus, horizontal MSE gradients are often thought to largely track moisture gradients associated with boundary layer temperature gradients in the deep tropics, and directly link to precipitation. This, however, cannot rule out the relevance of dry advection in the boundary layer, where the momentum budget has to be taken into account (Lindzen and Nigam 1987). Particularly when surface temperature gradients are strong, boundary layer convergence governed by momentum dynamics can produce shallow precipitating convection like that observed in the eastern Pacific ITCZ (Back and Bretherton 2006).

Hill et al. (2017) further advanced the MSE budget framework with an in-depth study of the MSE budget regulation over land, specifically over the Sahel during the West African monsoon's rainy season. They assess the impact of the convective parameterization and emergent convective depth on the climatological MSE budget regulation to explain the disparate projections of Sahel rainfall among climate models (e.g., Held et al. 2005). The present study takes a similar approach, but with an emphasis on the seasonal variations of the MSE budget regulation and thus the hydrological response to warming.

3. Results

a. Control climate

To determine whether the AM4 model is an appropriate tool for the questions of interest, we compare its control simulation of South American precipitation with the 1996–2015 observational record from the Global Precipitation Climatology Project (GPCP v2.3) (Adler et al. 2016). Figure 1a displays the precipitation seasonal cycle, averaged over the South American monsoon region (5°–18°S, 40°–72°W) and repeated to show all seasonal transitions. Across this domain, December–February (DJF) precipitation represents at least 30% of the annual mean, and in the core of the monsoon it exceeds 50%, as depicted in Fig. 5 of Silva and Kousky (2012) and Fig. 2 of Vuille et al. (2012). AM4 simulates the phase of precipitation with good fidelity to GPCP observations. The model-simulated dry austral winter season from June to August (JJA) exhibits rainfall rates below 1 mm day^{-1}. More vigorous precipitation develops in austral spring [September to November (SON)], producing a seasonal mean rainfall rate of 4.1 mm day^{-1}. Precipitation continues to intensify throughout austral summer (DJF), when the simulated monthly mean rainfall exceeds 11 mm day^{-1}. In austral fall [March–May (MAM)], the precipitation rate declines steadily toward 1 mm day^{-1}. The main shortcomings of the AM4 simulation are the wet bias in summer (maximum ~2 mm day^{-1}) and a more modest dry bias in winter, meaning a more rapid transition in spring than observed. By contrast, the CMIP3 model ensemble underestimates precipitation in all seasons (Torres and Marengo 2013). With such a severe and persistent dry bias, these models are prone to underestimate possible drying in warming experiments.

Besides its realistic seasonality, AM4 captures the spatial distribution of spring rainfall (the main focus of this work) reasonably well, with peak rainfall in the northwest and a distinct South Atlantic convergence zone (Fig. 1b). AM4 also realistically simulates the atmospheric flow over the region of

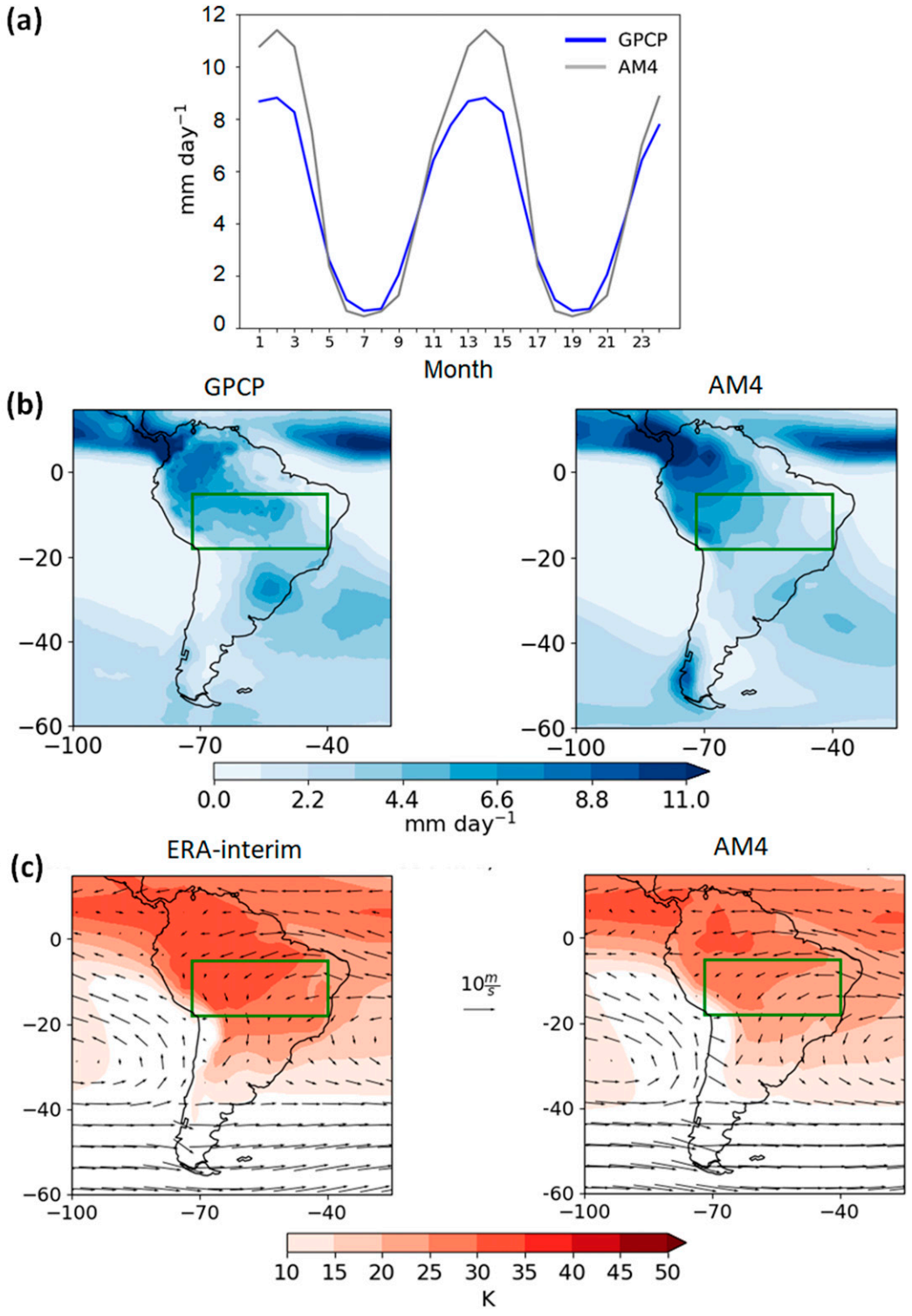

FIG. 1. (a) Seasonal cycle of region-mean precipitation over the South American monsoon sector [the area outlined in green in (b) and (c)] in GPCP v2.3 observations and AM4. Month 1 and month 13 represent the monthly mean value for January. The GPCP data are regridded to the AM4 horizontal resolution before spatial averaging. (b) Spring (SON) precipitation distribution in GPCP and AM4. (c) SON 850-hPa wind and moisture distributions in ERA-Interim and AM4. Moisture is expressed in terms of its contribution to MSE in K.

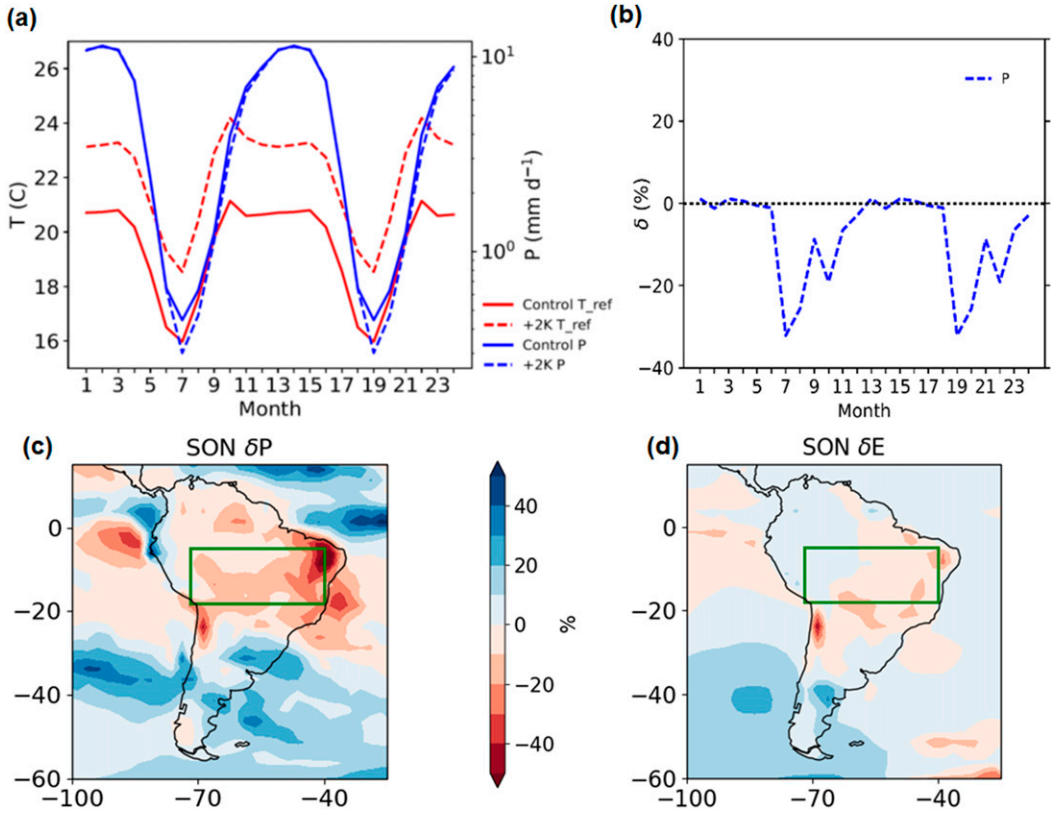

FIG. 2. (a) Seasonal cycles of precipitation and surface temperature over the South American monsoon sector based on the final 20 years of AM4 control and 2-K simulations. (b) Precipitation anomalies (2-K minus control) expressed as percentage of control values. (c) Spatial distribution of the spring precipitation anomalies (percentage). (d) As in (c), but for evaporation.

interest (Fig. 1c). Trade winds flow into the continent from the tropical Atlantic, supplying moisture. They further moisten over the rainforest due to strong evapotranspiration before being deflected by the Andes mountains into a meridional flow (Soares and Marengo 2009). It is also interesting to note that the boundary layer specific humidity is higher over the Amazon basin than over the Atlantic Ocean to the east (Fig. 1c), hinting at the important role of land surface processes in determining the land–ocean distribution of boundary layer moisture. At tropical latitudes, the simulated 850-hPa zonal moisture gradient is weaker than the ERA-Interim, with insufficient moisture over the Amazon basin (Fig. 1c). AM4 may therefore underestimate horizontal moisture advection across the monsoon sector, although the slightly stronger winds in AM4 compared to ERA-Interim somewhat compensate.

b. *Climate response to warming*

The seasonal cycles of precipitation and surface temperature in the 2-K warming experiment are contrasted with those in the control in Fig. 2a, with the percentage change in precipitation shown in Fig. 2b. The precipitation response is highly seasonally dependent. In the dry winter season, precipitation decreases by 0.10 mm day^{-1} from the climatological value of 0.57 mm day^{-1}, which amounts to a 17% decline. The drying is particularly severe in July and August (~30%). In spring, SST warming gives rise to a drying of 0.44 mm day^{-1} or 11%, and lowers the occurrence of precipitation at all intensities (not shown). Precipitation remains within 1% of control values in summer and fall. In contrast, the surface temperature response is largely consistent across all seasons. The average warming (~2.7 K) is greater than the prescribed SST warming (2 K).

The spring (SON) drying is coherent across the entire South American monsoon domain, and almost the entire continent north of ~30°S (Fig. 2c). The precipitation decreases by over 10% across the center of the monsoon domain and by over 20% along its eastern margin where rainfall is climatologically lower. Also of note is that the semiarid region of Northeast Brazil exhibits pronounced drying, in some places exceeding 40%. CMIP5 models and observations also predict that this region will grow more arid and drought-prone with global warming (e.g., Marengo and Bernasconi 2015). The strong drying signal extends east over the ocean between 10° and 20°S. By contrast, precipitation increases over most of the continent south of 30°S. We further examine this moistening signal in section 3c.

The vertical structures of some key properties in SON are plotted in Fig. 3. The free troposphere warms by more than 2 K in the 2-K experiment, and the warming generally increases

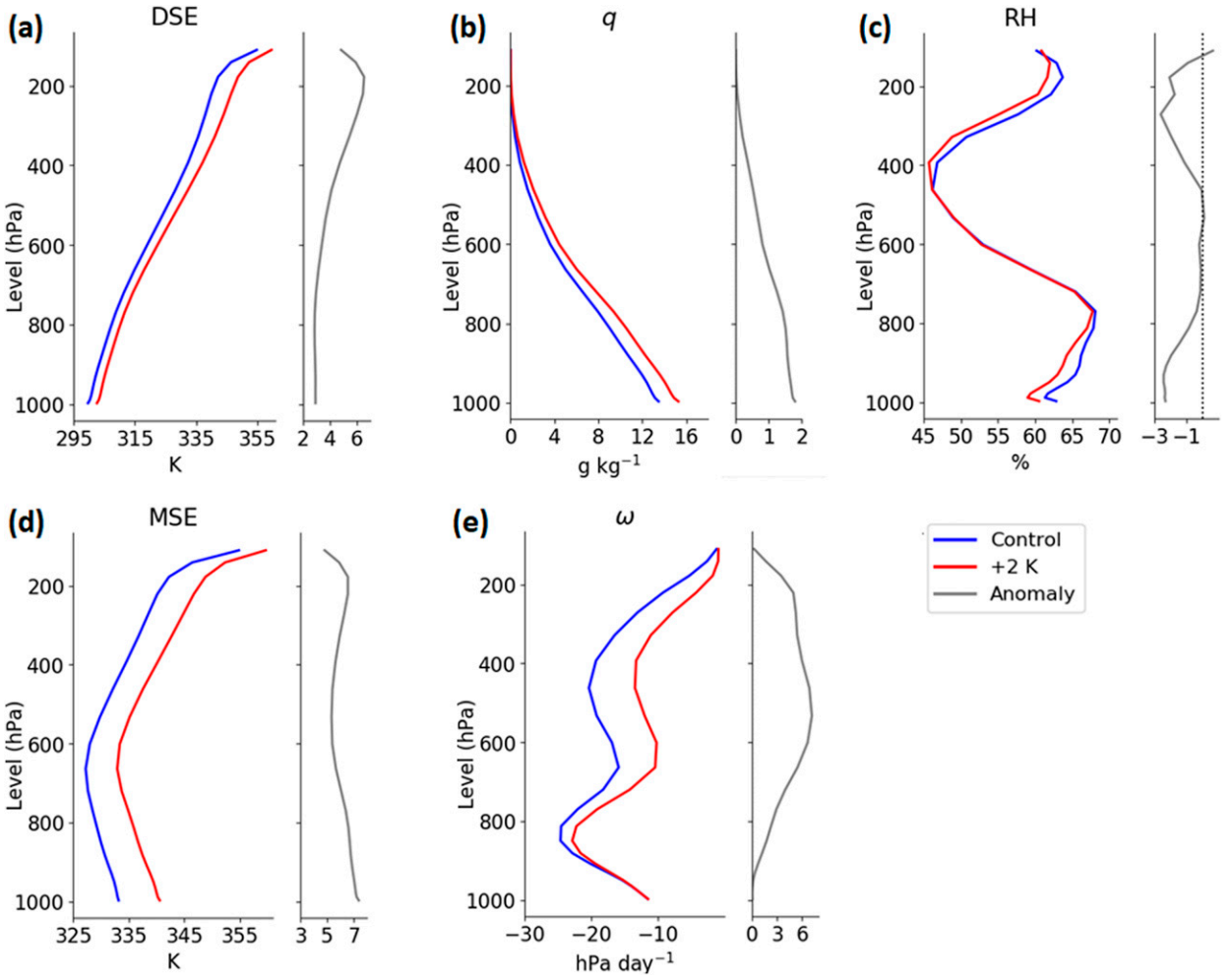

FIG. 3. Vertical profiles of SON region-mean (a) dry static energy (DSE), (b) specific humidity, (c) relative humidity, (d) MSE, and (e) vertical pressure velocity. For each variable, control values are blue, +2 K results are red, and anomalies (2-K minus control) are plotted on a separate axis in gray.

with height (e.g., ~4 K in the upper troposphere) as a direct consequence of the moist adiabatic control of the tropical lapse rate. Specific humidity also rises, most notably in the lower troposphere, where the relative increase is around 14%. This explains why relative humidity decreases slightly (from ~64% to ~61%); the rate at which specific humidity increases with temperature is less than 7% K^{-1}, the Clausius–Clapeyron scaling. Despite the small drop in relative humidity, the increase in MSE is rather uniform throughout the free troposphere, albeit accompanied by a modest steepening of the vertical gradient, suggesting that the region is still in convective quasi-equilibrium (Emanuel and Bretherton 1994). Consistent with the substantial reduction in precipitation, the large-scale ascent (ω) declines by up to ~30% (6 hPa day^{-1}) in the mid-troposphere. It is interesting to note that all three seasons characterized by mean climatological convection—spring, summer, and fall—exhibit anomalous descent in the 2-K SST warming experiment. In both summer and fall, the maximum descent anomaly is more modest at ~15% (not shown). Furthermore, while the weakening of ascent occurs in all three seasons, there is only a substantial precipitation reduction in spring.

The net precipitation (precipitation minus evaporation, or $P - E$) decreases by ~40% in spring, as opposed to only a few percent in summer and fall. Assuming steady state and a small role for horizontal advection in the moisture budget, one can approximate $P - E$ as $\{\overline{\omega}\,\partial\overline{q}/\partial p\}$. The ~40% $P - E$ reduction in spring is caused by the relatively large fractional change in $\overline{\omega}$ noted above. In summer and fall, the increase in boundary layer moisture and thus $\partial\overline{q}/\partial p$ is sufficient to maintain the control $P - E$ given the more modest weakening of convection.

In spring, the 2-K uniform SST perturbation causes warming by more than 2 K over land, exceeding 3 K along the southern boundary of the monsoon sector (Fig. 4a). This land-amplified warming results from the differing dry and moist adiabatic lapse rates operating over land and ocean respectively, combined with the constraint of weak temperature gradients in the free troposphere (Byrne and O'Gorman 2013). Specific humidity increases accompany the increased temperatures

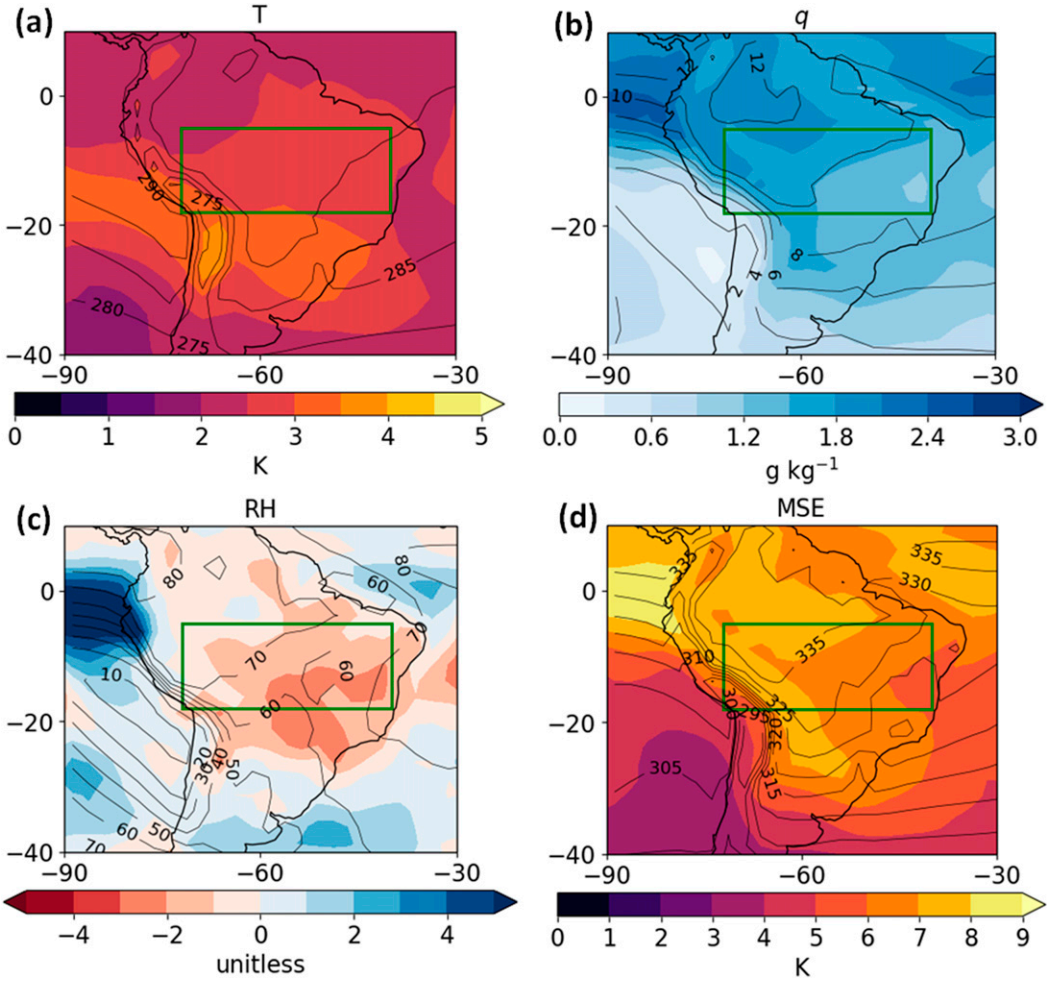

FIG. 4. Spatial distributions of SON 850-hPa controls (contours) and anomalies (2-K minus control; shading) of (a) temperature, (b) specific humidity, (c) relative humidity, and (d) MSE. The monsoon sector is outlined in green.

everywhere (Fig. 4b), but moisture limitations result in reduced low-level relative humidity across the land domain, particularly in the southeastern part of the monsoon sector (Fig. 4c). The anomalous boundary layer moist static energy distribution also reflects the combined effects of the temperature and moisture increases (Fig. 4d). The prevailing MSE gradient is enhanced, with MSE increasing by over 7 K to the northwest and along the Andes and by 4–5 K to the southeast. In the eastern monsoon sector, the enhanced zonal MSE gradient is associated with the anomalous temperature gradient, while the moisture response underlies the MSE pattern change in the west.

Overall, the 2-K SST warming simulation has a drier monsoon onset season in South America, supporting the conclusions of previous studies (e.g., Lau et al. 2013; Boisier et al. 2015; Biasutti and Sobel 2009; Seth et al. 2011). The present experiment demonstrates that uniform SST warming alone can drive this change in seasonality. As described in section 1, spring drying would strain the Amazon rainforest ecosystem. In the following section we investigate the cause of spring drying with the MSE budget.

c. *Mechanisms of drying*

To better understand the simulated spring drying, we examine the MSE budget regulation in the control experiment as well as its response to SST warming. The terms of the column-integrated MSE budget [Eq. (1)] are computed using the adjustment procedure of Hill et al. (2017, cf. their appendixes A and B). The eddy term is based on deviations from monthly means. Table 1 provides season- and region-mean values over the South American monsoon sector. In spring, $\overline{F}_{\text{net}}$ (69.5 W m^{-2}) is balanced primarily by horizontal MSE advection (37.9 W m^{-2}), with vertical advection (6.01 W m^{-2}) in a supporting role (Fig. 5, Table 1). Transient eddy MSE export completes the balance (22.0 W m^{-2}). This is a deviation from the Neelin and Held (1987) picture of precipitating tropical regions in which horizontal MSE advection is negligible. The vertical MSE advection term makes a larger relative contribution to column-integrated MSE export in the western half of the domain (Fig. 5b), where rainfall is stronger (Fig. 1b).

The leading-order balance of the perturbed SON MSE budget (2-K minus control) is between the horizontal and

TABLE 1. SON column-integrated MSE budget terms ($W\,m^{-2}$) in the control simulation, and anomalies (2-K minus control) averaged over the South American monsoon sector.

Term	Control	Anomaly
$\overline{F}_{net}$	69.5	−1.5
$\frac{\partial}{\partial t}\{\overline{\mathscr{E}}\}$	3.0	1.7
$\{\overline{\mathbf{v}}\cdot\nabla_p\overline{h}\}$	37.9	6.2
$\left\{\overline{\omega}\frac{\partial\overline{h}}{\partial p}\right\}$	6.0	−9.4
$\nabla\cdot\{\overline{h'\mathbf{v}'}\}$	22.0	−0.3

vertical advection terms, namely $\delta\{\overline{\omega}\,\partial\overline{h}/\partial p\} \approx -\delta\{\overline{\mathbf{v}}\cdot\nabla_p\overline{h}\}$, with the vertical contribution to MSE export reduced and the horizontal component enhanced (Fig. 6, Table 1). While the region remains moderately rainy (3.6 mm day^{-1}) in the 2-K warming experiment, the region-mean column-integrated vertical MSE advection turns into a net import ($-3.4\,W\,m^{-2}$), amounting to a negative GMS. Based on a linear decomposition, the increase in horizontal MSE advection (by $6.2\,W\,m^{-2}$) is almost entirely thermodynamic, associated with the climatological horizontal winds operating on the anomalous horizontal gradient of MSE: $\{\overline{\mathbf{v}}_{ctl}\cdot\delta\nabla_p\overline{h}\}$, where $\mathbf{v}_{ctl}$ is the control experiment horizontal wind vector (Fig. 1c). Due to the enhanced horizontal MSE gradient, the incursion of low MSE air by easterly inflow from the neighboring Atlantic Ocean more effectively ventilates the region in the 2-K warming experiment than in the control simulation. The enhanced horizontal MSE advection is primarily in the eastern part of the monsoon sector (Fig. 6a) where the anomalous MSE gradient (Fig. 4d) is most aligned with the zonal climatological flow (Fig. 1c).

We examine the separate contributions of dry static energy (DSE), $s = c_pT + gz$, and moisture terms (LE), $L_v q - L_f q_{ice}$, to the column-integrated MSE budget (Table 2). The $6.2\,W\,m^{-2}$ increase in region-mean horizontal MSE advection is due to the DSE component ($7.2\,W\,m^{-2}$), and offset only slightly by the moisture term. This is a distinction from the "upped-ante" mechanism described by Chou and Neelin (2004), which is

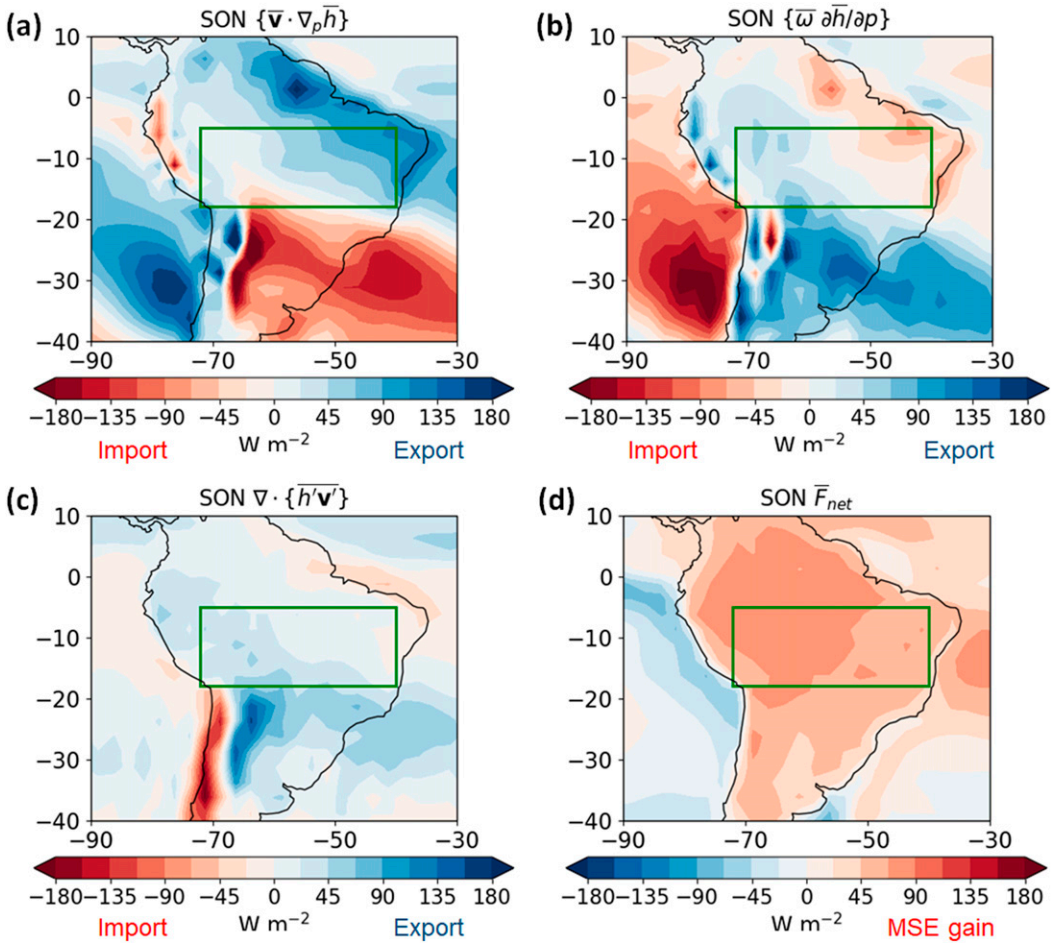

FIG. 5. Terms of the SON column-integrated MSE budget in the AM4 control simulation: (a) horizontal MSE advection, (b) vertical MSE advection, (c) transient eddy MSE flux divergence, and (d) net energetic forcing. Region mean values over the monsoon sector, outlined in green, are presented in Table 1.

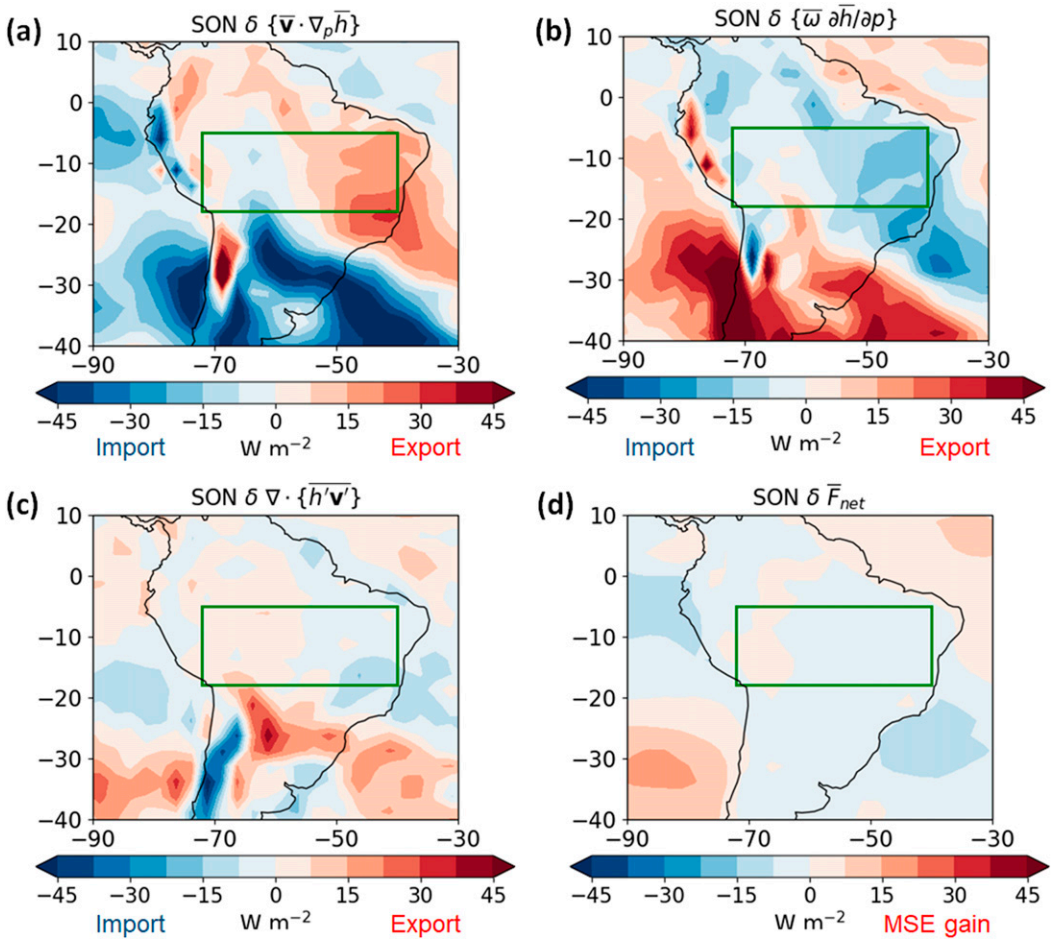

FIG. 6. Anomalies (2-K minus control) of the SON MSE budget terms: (a) horizontal MSE advection, (b) vertical MSE advection, (c) transient eddy MSE flux divergence, and (d) net energetic forcing. Region mean values over the monsoon sector, outlined in green, are presented in Table 1.

driven by anomalous moisture advection along convective margins. In the case of uniform warming on a well-watered surface, enhanced MSE gradients arise from the nonlinearity of the Clausius–Clapeyron relation: the specific humidity (q) increase per unit warming is higher at higher temperatures (Chou and Neelin 2004; Neelin et al. 2003; Boos and Hurley 2013). In the present 2-K warming experiment, by contrast, the enhanced warming over land compared to the adjacent Atlantic underlies the orientation of the anomalous MSE gradient in the eastern half of the monsoon domain, while the specific humidity anomaly is more uniform between land and ocean (Fig. 4). Relative humidity reductions are accordingly more pronounced in the east (Fig. 4c). Due to the warming pattern dictated by land geometry and surface properties, DSE advection increases thermodynamic ventilation of the South American monsoon sector in spring. While the MSE budget analysis alone indicates a common drying mechanism with that described by Chou and Neelin (2004), the subsequent decomposition demonstrates that local features can impact the relative importance of dry and moist processes. The prevalence of DSE advection as a tropical drying process has not previously been highlighted.

The anomalous MSE export via column-integrated horizontal advection elicits compensating import by the vertical advection. The control simulation ω profile exhibits two ascent peaks, at ~825 and ~450 hPa (Fig. 3e). In the 2-K experiment, anomalous subsidence throughout the column peaks near 500 hPa, reflecting weaker and shallower mean convection (Fig. 3e). As horizontal MSE gradients increase, column-integrated MSE is increasingly damped over the South American monsoon sector in spring, which is characteristic of substantial inflow up those gradients. In this way, barring compensating changes in eddies or F_{net}, regions can become less favorable for convection and exhibit weaker ascent and precipitation.

The MSE budget analysis informs a physical understanding of the regional precipitation response, but it does not foreclose the possibility that other processes, such as synoptic dynamics, also play a role. Analysis along these lines demonstrates that changes in the low-level horizontal flow field, in particular the low-level jet (LLJ), make a secondary contribution to the

TABLE 2. Decomposition of the SON column-integrated MSE budget terms (W m^{-2}) into dry static energy (DSE or s) and latent energy (LE) components in the control simulation, and anomalies (2-K minus control) averaged over the South American monsoon sector. Positive anomalies represent a greater contribution to MSE export.

Term	Control	Anomaly
$\{\overline{\mathbf{v}} \cdot \nabla_p \overline{s}\}$	16.7	7.2
$\{\overline{\mathbf{v}} \cdot \nabla_p \overline{\mathrm{LE}}\}$	21.4	−0.8
$\left\{\overline{\omega}\frac{\partial \overline{s}}{\partial p}\right\}$	85.1	−20.3
$\left\{\overline{\omega}\frac{\partial \overline{\mathrm{LE}}}{\partial p}\right\}$	−79.1	10.9
$\nabla \cdot \{\overline{s'\mathbf{v}'}\}$	2.5	−0.1
$\nabla \cdot \{\overline{\mathrm{LE}'\mathbf{v}'}\}$	19.2	−0.2

drying over the South American monsoon sector. A low-level jet is a meridional wind maximum in the lower 1–2 km of the atmosphere that forms to the east of a mountain barrier, in this case the Andes. This seasonally persistent synoptic feature transports moisture poleward from the Amazon to the La Plata river basin, feeding mesoscale convective systems there. A northerly LLJ regime causes low level moisture divergence over the Amazon and convergence and anomalous precipitation in the La Plata Basin (Wang and Fu 2004). As in two previous global warming simulation studies, in the 2-K experiment the LLJ strengthens in spring, as measured by the South American LLJ index: the mean 850-hPa meridional winds averaged over the region 15°–20°S, 65°–55°W (Wang and Fu 2004). In the 2-K experiment, the LLJ index northerlies strengthen by 0.8 m s^{-1} or 26% ($p < 0.001$) (Fig. 7a). This is consistent with the simulated precipitation increases south of ~30°S (Fig. 2c). The South American LLJ moisture transport is quantified as the region-mean meridional component of the column-integrated moisture flux $Q_\phi = \{\overline{q}\ \overline{v}\}$. In the 2-K experiment, the southward LLJ Q_ϕ increases by a magnitude of 35 kg s^{-1} m^{-1} or ~40% (Fig. 7b). As in previous studies, anomalous moisture transport by the LLJ exacerbates the spring season drying over the monsoon sector (Soares and Marengo 2009; Seth et al. 2010).

While in austral summer the LLJ is driven by local boundary layer processes, in other seasons, including spring, it is associated with upstream westerly winds that interact with the Andes and induce downstream cyclones via lee cyclogenesis (e.g., Wang and Fu 2004). In the AM4 2-K warming simulation, the SON Pacific subtropical high weakens, consistent with increased westerly flow over the Andes (Fig. 7a). Based on this dynamic mechanism, it is plausible that the strengthening of the LLJ, a synoptic feature, is driven by the broader changes in the large-scale subtropical circulation. Other features of the South American circulation, such as the South Atlantic convergence zone and the Bolivian high (not shown), show muted responses to uniform warming in spring.

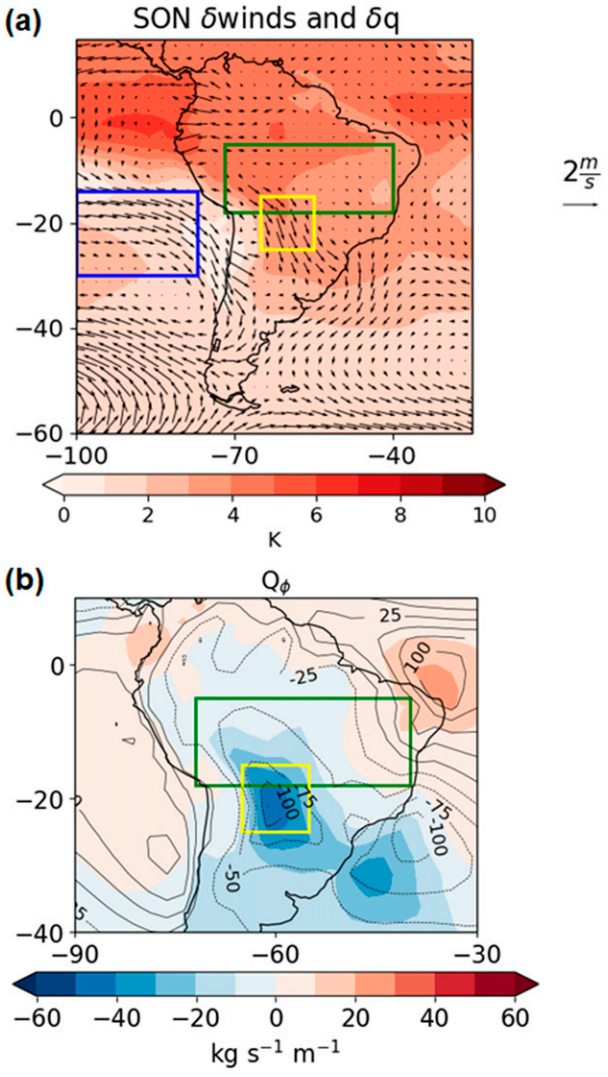

FIG. 7. (a) Anomalous (2-K minus control) SON winds and moisture at 850 hPa. The green box delimits the monsoon sector. The yellow box outlines the low-level jet sector, where winds are influenced by the strength of the westerlies in the region outlined in blue. (b) The SON column-integrated meridional moisture transport in the control (contours) and anomaly (shading).

4. Discussion

This study underscores that a uniform perturbation, in this case SST warming, can have uneven hydrological impacts in space and time. The analysis of the spring season response to SST warming enables us to diagnose a mechanism of drying in the South American monsoon sector. Comparing the climatological conditions and the precipitation response across all seasons allows us to identify the conditions that render one location or season more susceptible to drying than another. The results suggest that there are at least two necessary conditions for a significant precipitation reduction. The first condition is that the sector's climatological MSE ventilation is dominated by the horizontal, rather than the vertical, advection term. The second one is that the horizontal MSE advection increases in the perturbed climate. This provides a theoretical framework in which one can contrast spring with the other two

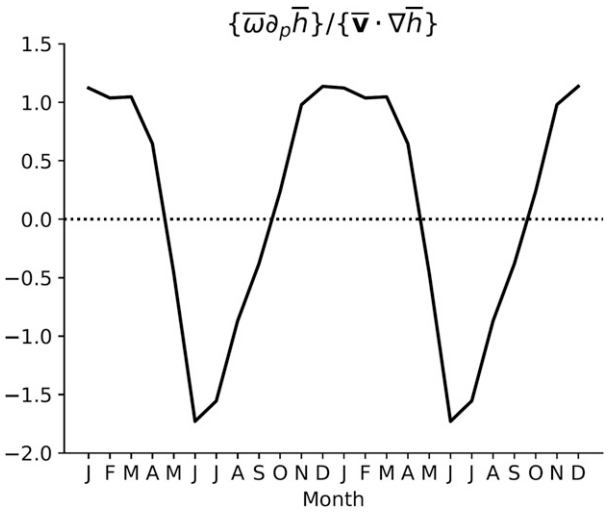

FIG. 8. Seasonal cycle of $V_{\mathrm{MSE}}/H_{\mathrm{MSE}}$ averaged over the South American monsoon sector in the control simulation.

raining seasons (summer and fall) to better understand the seasonal variations in the South American monsoon precipitation response.

The relative importance of vertical to horizontal MSE advection varies throughout the year, as reflected by the seasonal cycle of the climatological region-mean ratio $\{\overline{\omega}\,\partial\overline{h}/\partial p\}/\{\overline{\mathbf{v}}\cdot\nabla_p\overline{h}\}$ (Fig. 8). We abbreviate this ratio as $V_{\mathrm{MSE}}/H_{\mathrm{MSE}}$ for vertical and horizontal MSE advection. The column-integrated horizontal MSE advection is positive throughout the seasonal cycle, ventilating the region. By contrast, the vertical MSE advection contributes to export in the rainy season and import in the dry season. The $V_{\mathrm{MSE}}/H_{\mathrm{MSE}}$ ratio exceeds one in the summer rainy season, maximizing in December at 1.1, and minimizes in June at −1.7. In spring (SON), $V_{\mathrm{MSE}}/H_{\mathrm{MSE}}$ is small and positive (0.16), meaning that both terms contribute to column-integrated MSE export, with horizontal MSE advection dominating by a factor of approximately 6. In comparison, the fall season (MAM) has a $V_{\mathrm{MSE}}/H_{\mathrm{MSE}}$ of 0.51. Thus in both transition seasons, horizontal MSE advection trumps vertical advection in the column-integrated MSE export, although only by a factor of 2 in fall. However, the precipitation in fall is insensitive to SST warming, remaining within 1% of its control value of 6.9 mm day^{-1}, while it decreases substantially in spring. Why does the drying mechanism identified for spring, instigated by an increase in horizontal MSE advection, not occur in fall?

Emerging from the dry season, the control near-surface relative humidity in spring is ~60%, substantially lower than ~80% in fall, which follows the peak monsoon season. Under these humid conditions, the fall season does not exhibit the land–sea warming differential seen in spring (Fig. 4a), nor the associated anomalous zonal MSE gradient between the South American landmass and the Atlantic Ocean (Fig. 4d). Instead, the fall season anomalous MSE gradient is predominantly meridional. Accordingly, the easterly winds flowing onto the continent do not operate on the anomalous MSE gradient, impeding the thermodynamic drying mechanism which operates effectively in spring. A linear decomposition confirms that there is minimal change in $\{\overline{\mathbf{v}_{\mathrm{ctl}}}\cdot\delta\nabla_p\overline{h}\}$ due to SST warming; the change in horizontal MSE advection in fall is almost entirely due to dynamic changes that advect relatively high MSE air into the region. In other words, the fall season does not satisfy the second condition for drying. Seasonal differences in land surface conditions, namely the moisture availability, play a key role in the distinct spring and fall hydrological responses to warming.

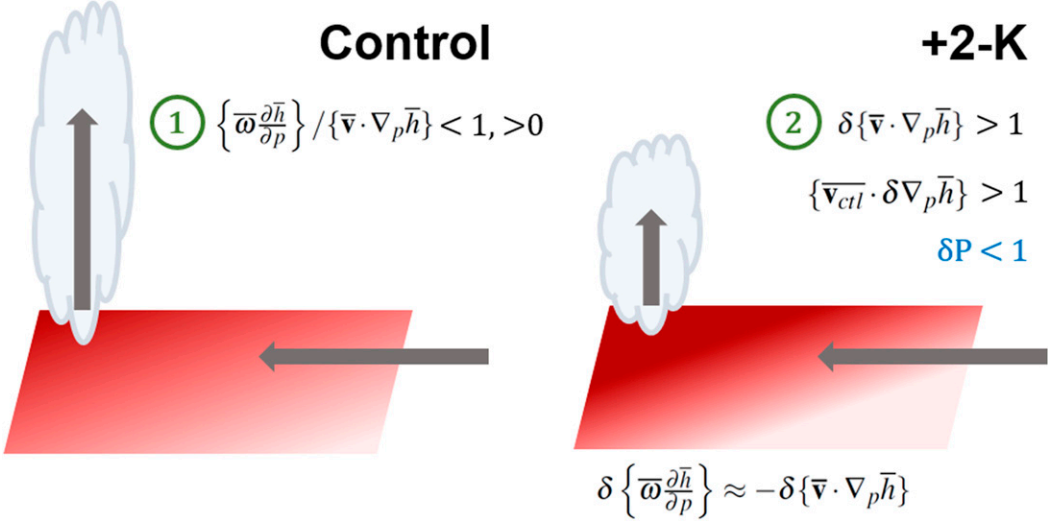

FIG. 9. A depiction of the thermodynamic drying mechanism, with arrows representing mean winds and the red gradient indicating the MSE distribution. A region is susceptible to drying when the two criteria are satisfied: the climatological region-mean ratio of $V_{\mathrm{MSE}}/H_{\mathrm{MSE}}$ is positive and less than one, and the horizontal MSE advection increases in the perturbed climate. In the warmer climate, the mean winds act on enhanced horizontal MSE gradients, ventilating the monsoon sector and inhibiting convection and precipitation.

In summer (the peak rainy season), the horizontal MSE advection increases by $\sim 4\,\mathrm{W\,m^{-2}}$ in the 2-K experiment, but this does not suppress precipitation. A possible reason is that summer does not satisfy the first condition for drying: the DJF $V_{\mathrm{MSE}}/H_{\mathrm{MSE}}$ ratio is > 1, implying a secondary role for horizontal advection in column-integrated MSE discharge, and thus reduced sensitivity to the enhanced horizontal MSE gradients. The monsoonal precipitation is driven by sufficiently vigorous and top-heavy convection that it withstands modest increases in the horizontal MSE advection.

5. Conclusions

In the GFDL AM4 model, uniform SST warming causes significant rainfall reductions in the South American monsoon onset season (spring). Several studies based on observations and comprehensive climate model simulations also conclude that climate change will impede spring precipitation in the monsoon sector (e.g., Lau et al. 2013; Boisier et al. 2015; Biasutti and Sobel 2009; Seth et al. 2011; Wang et al. 2020). The present analysis demonstrates that this change in seasonality is linked to the uniform warming component of greenhouse gas–induced climate change. The prospect of diminishing rainforests due to such a change in seasonality is of global concern due to the Amazon's unparalleled biodiversity and its major role in the carbon cycle.

The MSE budget is a useful theoretical framework for systematically diagnosing the mechanisms of precipitation change over land. The seasonal cycle of $V_{\mathrm{MSE}}/H_{\mathrm{MSE}}$ encapsulates the time-varying MSE budget regulation in the climatology. Based on the climatological MSE regime, one can identify regions and seasons in which rainfall is likely resilient to the impacts of SST warming, and those where precipitation is subject to change. Convective regions where horizontal MSE advection dominates the climatological MSE budget are prone to drying, but only do so if horizontal MSE advection increases in the perturbed climate (Fig. 9). The comparison of South American spring and fall illustrates that the horizontal MSE advection response is influenced by the land geometry and surface water availability, which together determine the anomalous MSE pattern. Continued research to elucidate the seasonally varying influence of surface conditions on the hydrological response to warming will bolster regional climate projections.

Further study of simulations with different climate perturbations, such as realistic greenhouse gas or aerosol forcing, will be useful to identify additional mechanisms of and conditions for precipitation change. The impact of SST warming on the full probability distribution of precipitation also warrants further study (e.g., Norris et al. 2019). The focus here on the mean precipitation response to uniform SST warming facilitates interpretation of certain robust impacts of climate change. The results provide valuable physical insights to better understand how increasing temperatures could cause severe drying in the South American monsoon onset season.

Acknowledgments. Thanks to Ming Zhao for providing the GFDL AM4 model simulations. We also thank Spencer Hill and Spencer Clark, developers of the ''aospy'' climate model analysis package for Python.

REFERENCES

Adam, O., T. Bischoff, and T. Schneider, 2016: Seasonal and interannual variations of the energy flux equator and ITCZ. Part II: Zonally varying shifts of the ITCZ. *J. Climate*, **29**, 7281–7293, https://doi.org/10.1175/JCLI-D-15-0710.1.

Adler, R., and Coauthors, 2016: The new version 2.3 of the Global Precipitation Climatology Project (GPCP) monthly analysis product. University of Maryland, April, 1072–1084.

Back, L., and C. Bretherton, 2006: Geographic variability in the export of moist static energy and vertical motion profiles in the tropical Pacific. *Geophys. Res. Lett.*, **33**, L17810, https://doi.org/10.1029/2006GL026672.

Biasutti, M., and A. H. Sobel, 2009: Delayed Sahel rainfall and global seasonal cycle in a warmer climate. *Geophys. Res. Lett.*, **36**, L23707, https://doi.org/10.1029/2009GL041303.

——, ——, and S. Camargo, 2009: The role of the Sahara low in summertime Sahel rainfall variability and change in the CMIP3 models. *J. Climate*, **22**, 5755–5771, https://doi.org/10.1175/2009JCLI2969.1.

——, and Coauthors, 2018: Global energetics and local physics as drivers of past, present and future monsoons. *Nat. Geosci.*, **11**, 392–400, https://doi.org/10.1038/s41561-018-0137-1.

Boisier, J., P. Ciais, A. Ducharne, and M. Guimberteau, 2015: Projected strengthening of Amazonian dry season by constrained climate model simulations. *Nat. Climate Change*, **5**, 656–660, https://doi.org/10.1038/nclimate2658.

Boos, W. R., and J. V. Hurley, 2013: Thermodynamic bias in the multimodel mean boreal summer monsoon. *J. Climate*, **26**, 2279–2287, https://doi.org/10.1175/JCLI-D-12-00493.1.

——, and R. Korty, 2016: Regional energy budget control of the intertropical convergence zone and application to mid-Holocene rainfall. *Nat. Geosci.*, **9**, 892–897, https://doi.org/10.1038/ngeo2833.

Byrne, M. P., and P. A. O'Gorman, 2013: Land–ocean warming contrast over a wide range of climates: Convective quasi-equilibrium theory and idealized simulations. *J. Climate*, **26**, 4000–4016, https://doi.org/10.1175/JCLI-D-12-00262.1.

——, and ——, 2015: The response of precipitation minus evapotranspiration to climate warming: Why the ''wet-get-wetter, dry-get-drier'' scaling does not hold over land. *J. Climate*, **28**, 8078–8092, https://doi.org/10.1175/JCLI-D-15-0369.1.

Cess, R. D., and Coauthors, 1990: Intercomparison and interpretation of climate feedback processes in 19 atmospheric general circulation models. *J. Geophys. Res.*, **95**, 16 601–16 615, https://doi.org/10.1029/JD095iD10p16601.

Chadwick, R., 2016: Which aspects of CO_2 forcing and SST warming cause most uncertainty in projections of tropical rainfall change over land and ocean? *J. Climate*, **29**, 2493–2509, https://doi.org/10.1175/JCLI-D-15-0777.1.

Charney, J. G., 1963: A note on large-scale motions in the tropics. *J. Atmos. Sci.*, **20**, 607–609, https://doi.org/10.1175/1520-0469(1963)020<0607:ANOLSM>2.0.CO;2.

Chou, C., and J. D. Neelin, 2004: Mechanisms of global warming impacts on regional tropical precipitation. *J. Climate*, **17**, 2688–2701, https://doi.org/10.1175/1520-0442(2004)017<2688:MOGWIO>2.0.CO;2.

——, and C.-W. Lan, 2012: Changes in the annual range of precipitation under global warming. *J. Climate*, **25**, 222–235, https://doi.org/10.1175/JCLI-D-11-00097.1.

Dwyer, J. G., M. Biasutti, and A. H. Sobel, 2014: The effect of greenhouse gas–induced changes in SST on the annual cycle of zonal mean tropical precipitation. *J. Climate*, **27**, 4544–4565, https://doi.org/10.1175/JCLI-D-13-00216.1.

Emanuel, K. A., 1995: On thermally direct circulations in moist atmospheres. *J. Atmos. Sci.*, **52**, 1529–1534, https://doi.org/10.1175/1520-0469(1995)052<1529:OTDCIM>2.0.CO;2.

——, J. D. Neelin, and C. S. Bretherton, 1994: On large-scale circulations in convecting atmospheres. *Quart. J. Roy. Meteor. Soc.*, **120**, 1111–1143, https://doi.org/10.1002/qj.49712051902.

Fu, R., and W. Li, 2004: The influence of the land surface on the transition from dry to wet season in Amazonia. *Theor. Appl. Climatol.*, **78**, 97–110, https://doi.org/10.1007/s00704-004-0046-7.

——, and Coauthors, 2013: Increased dry-season length over southern Amazonia in recent decades and its implication for future climate projection. *Proc. Natl. Acad. Sci. USA*, **110**, 18 110–18 115, https://doi.org/10.1073/PNAS.1302584110.

Giannini, A., R. Saravanan, and P. Chang, 2003: Oceanic forcing of Sahel rainfall on interannual to interdecadal time scales. *Science*, **302**, 1027–1030, https://doi.org/10.1126/science.1089357.

He, J., B. J. Soden, and B. Kirtman, 2014: The robustness of the atmospheric circulation and precipitation response to future anthropogenic surface warming. *Geophys. Res. Lett.*, **41**, 2614–2622, https://doi.org/10.1002/2014GL059435.

Heaviside, C., and A. Czaja, 2013: Response of the African monsoon to orbital forcing and ocean feedbacks in the middle Holocene. *Quart. J. Roy. Meteor. Soc.*, **139**, 2181–2189, https://doi.org/10.1002/qj.2085.

Held, I., T. Delworth, J. Lu, K. Findell, and T. Knutson, 2005: Simulation of Sahel drought in the 20th and 21st centuries. *Proc. Natl. Acad. Sci. USA*, **102**, 17 891–17 896, https://doi.org/10.1073/pnas.0509057102.

Hill, S. A., 2019: Theories for past and future monsoon rainfall changes. *Curr. Climate Change Rep.*, **5**, 160–171, https://doi.org/10.1007/S40641-019-00137-8.

——, Y. Ming, and I. Held, 2015: Mechanisms of forced tropical meridional energy flux change. *J. Climate*, **28**, 1725–1742, https://doi.org/10.1175/JCLI-D-14-00165.1.

——, ——, ——, and M. Zhao, 2017: A moist static energy budget–based analysis of the Sahel rainfall response to uniform oceanic warming. *J. Climate*, **30**, 5637–5660, https://doi.org/10.1175/JCLI-D-16-0785.1.

Huang, P., S.-P. Xie, K. Hu, G. Huang, and R. Huang, 2013: Patterns of the seasonal response of tropical rainfall to global warming. *Nat. Geosci.*, **6**, 357–361, https://doi.org/10.1038/ngeo1792.

Hurley, J., and W. Boos, 2013: Interannual variability of monsoon precipitation and local subcloud equivalent potential temperature. *J. Climate*, **26**, 9507–9527, https://doi.org/10.1175/JCLI-D-12-00229.1.

Jones, C., and L. M. Carvalho, 2013: Climate change in the South American monsoon system: Present climate and CMIP5 projections. *J. Climate*, **26**, 6660–6678, https://doi.org/10.1175/JCLI-D-12-00412.1.

Kang, S., I. Held, D. Frierson, and M. Zhao, 2008: The response of the ITCZ to extratropical thermal forcing: Idealized slab-ocean experiments with a GCM. *J. Climate*, **21**, 3521–3532, https://doi.org/10.1175/2007JCLI2146.1.

Kent, C., R. Chadwick, and D. Rowell, 2015: Understanding uncertainties in future projections of seasonal tropical precipitation. *J. Climate*, **28**, 4390–4413, https://doi.org/10.1175/JCLI-D-14-00613.1.

Kintisch, E., 2015: Amazon rainforest ability to soak up carbon dioxide is falling. *Science*, accessed September 2019, https://doi.org/10.1126/science.aab0336.

Lau, W. K.-M., H.-T. Wu, and K.-M. Kim, 2013: A canonical response of precipitation characteristics to global warming from CMIP5 models. *Geophys. Res. Lett.*, **40**, 3163–3169, https://doi.org/10.1002/grl.50420.

Lee, J.-Y., and B. Wang, 2014: Future change of global monsoon in the CMIP5. *Climate Dyn.*, **42**, 101–119, https://doi.org/10.1007/s00382-012-1564-0.

Li, W., R. Fu, and R. E. Dickinson, 2006: Rainfall and its seasonality over the amazon in the 21st century as assessed by the coupled models for the IPCC AR4. *J. Geophys. Res.*, **111**, D02111, https://doi.org/10.1029/2005JD006355.

Lindzen, R. S., and S. Nigam, 1987: On the role of sea surface temperature gradients in forcing low-level winds and convergence in the tropics. *J. Atmos. Sci.*, **44**, 2418–2436, https://doi.org/10.1175/1520-0469(1987)044<2418:OTROSS>2.0.CO;2.

Lu, J., and T. L. Delworth, 2005: Oceanic forcing of the late 20th century Sahel drought. *Geophys. Res. Lett.*, **32**, L22706, https://doi.org/10.1029/2005GL023316.

Marengo, J. A., and M. Bernasconi, 2015: Regional differences in aridity/drought conditions over northeast Brazil: Present state and future projections. *Climatic Change*, **129**, 103–115, https://doi.org/10.1007/s10584-014-1310-1.

Muller, C., and P. O'Gorman, 2011: An energetic perspective on the regional response of precipitation to climate change. *Nat. Climate Change*, **1**, 266–271, https://doi.org/10.1038/nclimate1169.

Neelin, J. D., 2007: Moist dynamics of tropical convection zones in monsoons, teleconnections, and global warming. *The Global Circulation of the Atmosphere*, A. Sobel and T. Schneider, Eds., Princeton University Press, 267–301.

——, and I. Held, 1987: Modeling tropical convergence based on the moist static energy budget. *Mon. Wea. Rev.*, **115**, 3–12, https://doi.org/10.1175/1520-0493(1987)115<0003:MTCBOT>2.0.CO;2.

——, C. Chou, and H. Su, 2003: Tropical drought regions in global warming and El Niño teleconnections. *Geophys. Res. Lett.*, **30**, 2275, https://doi.org/10.1029/2003GL018625.

Norris, J., G. Chen, and J. D. Neelin, 2019: Thermodynamic versus dynamic controls on extreme precipitation in a warming climate from the Community Earth System Model large ensemble. *J. Climate*, **32**, 1025–1045, https://doi.org/10.1175/JCLI-D-18-0302.1.

Privé, N. C., and R. A. Plumb, 2007: Monsoon dynamics with interactive forcing. Part I: Axisymmetric studies. *J. Atmos. Sci.*, **64**, 1417–1430, https://doi.org/10.1175/JAS3916.1.

Ruffato-Ferreira, V., R. da Costa Barreto, A. O. Júnior, W. L. Silva, D. de Berrêdo Viana, J. A. S. do Nascimento, and M. A. V. de Freitas, 2017: A foundation for the strategic long-term planning of the renewable energy sector in Brazil: Hydroelectricity and wind energy in the face of climate change scenarios. *Renew. Sustain. Energy Rev.*, **72**, 1124–1137, https://doi.org/10.1016/j.rser.2016.10.020.

Schneider, T., T. Bischoff, and G. Huag, 2014: Migrations and dynamics of the intertropical convergence zone. *Nature*, **513**, 45–53, https://doi.org/10.1038/nature13636.

Seth, A., M. Rojas, and S. A. Rauscher, 2010: CMIP3 projected changes in the annual cycle of the South American monsoon. *Climatic Change*, **98**, 331–357, https://doi.org/10.1007/s10584-009-9736-6.

——, S. A. Rauscher, M. Rojas, A. Giannini, and S. J. Camargo, 2011: Enhanced spring convective barrier for monsoons in a warmer world? *Climatic Change*, **104**, 403–414, https://doi.org/10.1007/s10584-010-9973-8.

——, ——, M. Biasutti, A. Giannini, S. J. Camargo, and M. Rojas, 2013: CMIP5 projected changes in the annual cycle of precipitation in monsoon regions. *J. Climate*, **26**, 7328–7351, https://doi.org/10.1175/JCLI-D-12-00726.1.

——, A. Giannini, S. Rauscher, S. Bordoni, D. Singh, and S. Camargo, 2019: Monsoon responses to climate changes—Connecting

past, present and future. *Curr. Climate Change Rep.*, **5**, 63–79, https://doi.org/10.1007/s40641-019-00125-y.

Silva, V. B., and V. E. Kousky, 2012: The South American monsoon system: Climatology and variability. *Modern Climatology*, S. Wang and R. Gillies, Eds., InTech, 5–152.

Smyth, J., S. Hill, and Y. Ming, 2018: Simulated responses of the West African monsoon and zonal-mean tropical precipitation to early Holocene orbital forcing. *Geophys. Res. Lett.*, **45**, 12 049–12 057, https://doi.org/10.1029/2018GL080494.

Soares, W. R., and J. A. Marengo, 2009: Assessments of moisture fluxes east of the Andes in South America in a global warming scenario. *Int. J. Climatol.*, **29**, 1395–1414, https://doi.org/10.1002/JOC.1800.

Taylor, K. E., D. Williamson, and F. Zwiers, 2000: The sea surface temperature and sea-ice concentration boundary conditions for AMIP II simulations. PCMDI Rep. 60, 28 pp., https://pcmdi.llnl.gov/report/ab60.html.

Torres, R. R., and J. A. Marengo, 2013: Uncertainty assessments of climate change projections over South America. *Theor. Appl. Climatol.*, **112**, 253–272, https://doi.org/10.1007/s00704-012-0718-7.

Vera, C., and Coauthors, 2006: The South American Low-Level Jet Experiment. *Bull. Amer. Meteor. Soc.*, **87**, 63–78, https://doi.org/10.1175/BAMS-87-1-63.

Vuille, M., and Coauthors, 2012: A review of the South American monsoon history as recorded in stable isotopic proxies over the past two millennia. *Climate Past*, **8**, 1309–1321, https://doi.org/10.5194/cp-8-1309-2012.

Wang, B., C. Jin, and J. Liu, 2020: Understanding future change of global monsoons projected by CMIP6 models. *J. Climate*, **33**, 6471–6489, https://doi.org/10.1175/JCLI-D-19-0993.1.

Wang, H., and R. Fu, 2004: Influence of cross-Andes flow on the South American low-level jet. *J. Climate*, **17**, 1247–1262, https://doi.org/10.1175/1520-0442(2004)017<1247:IOCFOT>2.0.CO;2.

Xie, S.-P., and Coauthors, 2015: Towards predictive understanding of regional climate change. *Nat. Climate Change*, **5**, 921–930, https://doi.org/10.1038/nclimate2689.

Zhao, M., and Coauthors, 2018a: The GFDL global atmosphere and land model AM4.0/LM4.0: 1. Simulation characteristics with prescribed SSTs. *J. Adv. Model. Earth Syst.*, **10**, 691–734, https://doi.org/10.1002/2017MS001208.

——, and Coauthors, 2018b: The GFDL global atmosphere and land model AM4.0/LM4.0: 2. Model description, sensitivity studies, and tuning strategies. *J. Adv. Model. Earth Syst.*, **10**, 735–769, https://doi.org/10.1002/2017MS001209.